2007

Fast-Scan Cyclic Voltammetry - Scanning Electrochemical Microscopy

Luis Díaz-Ballote
(CINVESTAV-IPN), Unidad Mérida,, luisdiaz@mda.cinvestav.mx

Mario A. Apuche-Avlles

David O. Wipf
Mississippi State University, dow1@msstate.edu

Fast-Scan Cyclic Voltammetry - Scanning Electrochemical Microscopy

Luis Díaz-Ballote[1], Mario Alpuche-Aviles[2], and David O. Wipf*

Department of Chemistry

Mississippi State University

Mississippi State MS 39762

wipf@ra.msstate.edu

This accepted manuscript was published as Luis Díaz-Ballote, Mario Alpuche-Aviles, David O. Wipf, Fast-scan cyclic voltammetry–scanning electrochemical microscopy, Journal of Electroanalytical Chemistry, Volume 604, Issue 1, 2007, Pages 17-25, https://doi.org/10.1016/j.jelechem.2007.02.023

ABSTRACT

The use of fast scan cyclic voltammetry (FSCV) to generate images in scanning electrochemical microscopy is demonstrated. In the FSCV-SECM method a cyclic voltammogram is acquired at each grid point of the scanned area. Thus, each point in the SECM image is a data array rather than a single value. This provides a significant increase in the amount of data collected per scan and provides the ability to make images of multiple analytes per scan. In addition, the use of cyclic voltammetry allows images based on adsorptive as well as diffusional processes. In this paper, we describe the FSCV-SECM experiment and equipment, we show that FSCV-SECM can resolve multiple chemical species in a single scan, and we demonstrate that cathodic-stripping voltammetry can be used to image the concentration profiles of halide ions.

Keywords: Scanning Electrochemical Microscopy, Ultramicroelectrodes, Cyclic Voltammetry, Stripping Voltammetry

[1] Present Address: Applied Physics Department, Center for Investigation and Advanced Study (CINVESTAV-IPN), Unidad Mérida, AP 73 Cordemex, Mérida, Yucatan, 97310, México, luisdiaz@mda.cinvestav.mx

[2] Present Address: Department of Chemistry and Biochemistry University of Texas at Austin, 1 University Station A5300 Austin, TX 78712-0165, malpuche@mail.utexas.edu

INTRODUCTION

The scanning electrochemical microscope is a scanned-probe method operating in an electrolyte solution [1]. The scanning probe is an ultramicroelectrode tip with micrometer or smaller dimension. By rastering the probe in close proximity to the surface of the sample, a map is made of the electrochemical response of the microelectrode tip. The origin of active interest in the area is marked by the introduction of feedback SECM by Bard and coworkers [2, 3] and the earlier work by Engstrom [4, 5] on what would come to be known as the generation-collection SECM mode. In these studies, and in all subsequent work, image maps formed by SECM are based on a single amperometric or potentiometric [6-8] measurement of the probe signal as a function of the tip position. Data are generally presented as a two-dimensional projection map of the tip signal as a function of two spatial coordinates. In the various literature reports that describe SECM instrumentation and its principles, the tip signal is, or is assumed to be, steady-state [9-14].

SECM imaging experiments are usually classified as either feedback or generation-collection (GC) [1, 15]. The feedback imaging mode uses a mediator species (often intentionally added to the solution) as a method to examine the surface topography and electrochemical reactivity of the surface. In GC imaging, the tip is used as a chemical sensor. Images are constructed by scanning the tip near the surface and recording the tip signal. Potentiometric (ion selective electrodes, ISE) tips are used to provide selective determination of a single ionic species. Amperometric tips can analyze any number of redox active compounds but selectivity is poor and the response is difficult to interpret in unknown or complex mixtures.

An alternate method for SECM is suggested by the properties of the amperometric ultramicroelectrode tip. The size of the ultramicroelectrode tip makes them ideal for rapid voltammetric measurements due to their small ohmic drop and double-layer capacitance [16, 17].

As an example, consider that amperometric microelectrodes are now commonly used for *in-vivo* study of neurochemical processes by using fast scan cyclic voltammetry (FSCV) [18, 19]. In many respects the original concerns that lead to the adoption of FSCV in neuroelectrochemistry are mirrored in SECM. FSCV increases selectivity and the use of rapid scans allows study of rapidly changing concentration profiles by allowing short, repetitive measurements [20-22]. FSCV can also greatly increase sensitivity for materials that adsorb at the electrode [21, 23, 24]. In this paper we show that there are several advantages to combining FSCV with SECM imaging (FSCV-SECM).

For distinction, we use the term *amperometric SECM* (A-SECM) when the tip is used as an amperometric sensor and *voltammetric SECM* (V-SECM) when the tip is used as a voltammetric sensor. There are several important distinctions between V-SECM and A-SECM. The first is the increased selectivity afforded by the voltammetric potential excitation. The use of a potential sweep allows essentially simultaneous measurements at all potentials in the sweep permitting V-SECM to image multiple chemical species by differences in formal potentials. In contrast, only a single current-potential pair is recorded per tip position in A-SECM. This limitation makes A-SECM measurements in complex systems (i.e. more than a single redox component) difficult to unambiguously interpret. By linking a voltammetric sweep with SECM imaging, a new dimension of imaging modes are made possible. For example, images based on adsorption can be made—not only for redox active adsorbates (e.g. cathodic stripping voltammetry) but for non-redox active species by plotting changes in double-layer capacitance with tip position. With cyclic voltammetry-SECM, chemically based imaging modes can be implemented that employ changes in peak position or amplitude due to various localized chemical effects, such as the presence of complexing agents or other reactive species, pH changes, changes in ionic strength (e.g. iR drop or ion-pairing effects), and adsorbates.

In this report, we describe the FSCV-SECM instrument and demonstrate how steady-state and CV transient currents are used to develop unique chemical concentration maps. Using fast CV scan rates, the time to acquire a CV is essentially negligible compared to the time required to move the tip. Thus, imaging times are equivalent to normal A-SECM imaging times. The ability to discriminate complex systems species using FSCV-SECM is shown by examination of the concentration profiles of the reactants and products found above a microelectrode substrate during the ECE reaction of acetaminophen (N-acetyl-p-aminophenol, APAP). In addition, the use of cyclic voltammetry allows images based on adsorptive as well as diffusional processes and this is demonstrated by using cathodic stripping voltammetry to produce concentration profiles of chloride ion generated during the reduction of trichloroacetic acid (TCA).

EXPERIMENTAL PROCEDURE

Imaging tips and substrates were 10 to 100-μm diam Pt and Au disks, glass insulated and built as described previously by sealing Pt and Au wires (Goodfellow Metals, Ltd., Cambridge, UK) into soft glass [17, 25]. Substrate electrodes were potted in EPON 828 epoxy (Miller-Stephenson, Danbury, CT) with 13 wt% triethylenetetramine hardener (Miller-Stephenson). A microdisk electrode was exposed by grinding with 320, 600, and 1500 grit SiC paper and then polished with alumina abrasives down to 0.05 μm. Hg-coated Pt electrodes were prepared by polishing the Pt electrode with 0.3 μm alumina and depositing a Hg film by using 90 cyclic voltammetry scans at 50 V/s from 0 and –790 mV vs. MSE in a solution of 5.7 mM $HgNO_3$, 1.0 M KNO_3, 0.5 % v/v conc. HNO_3. The electrodes were inspected by optical microscopy to ensure the formation of complete, thin Hg film on the Pt surface.

Acetaminophen (4-acetamidophenol, 98 % Aldrich, Milwaukee WI), and *N*,*N*-dimethyl-1,4-phenylenediamine (97 % Aldrich, Milwaukee WI) and trichloroacetic acid (TCA) were used without further purification. All other chemicals were reagent grade and solutions were prepared

with distilled-deionized water (18.2 MΩ-cm). Potentials are reported vs either Ag/AgCl in 3 M KCl or $Hg/HgSO_4$ in saturated K_2SO_4 (MSE). Solutions of trichloroacetic acid (TCA) were prepared in pH 7.2 McIlvaine buffer solution: 165 mM Na_2HPO_4, 1.8 mM citric acid. Chloride standard solutions were prepared from a KCl stock solution.

Instrumentation The FSCV-SECM instrument is a modified version of previously described systems [26, 27]. During acquisition of a line scan, the SECM program follows the timing diagram shown in Figure 1. Collection of a set of data involves repetition of a sequence of three steps: tip movement, amperometric data collection, and voltammetric data collection. A tip movement requires about 100-1000 ms, depending on the speed and desired spatial resolution. After *tip movement*, amperometric information is acquired (*A-SECM Acq*). This data is the tip current measured at a fixed voltage corresponding to the initial voltage prior to the cyclic voltammogram and is used to generate an A-SECM GC image. In addition, up to six additional auxiliary channels are recorded at this point, for example, any signals for the substrate current or potential, topography, and conductivity.

After the amperometric data is acquired and prior to the next movement step, the voltammetric signal is recorded (Figure 1). To avoid objectionable introduction of excess noise into the image, the voltammetric sweep is phase locked to the ac power signal. Since noise spikes on the power line signal (*Mains Current*) are highly correlated to the power phase, synchronized sampling of the analog signal (*Tip Current*) to the power-line phase locates the noise at the same potential or time on all the voltammograms. If synchronization is not used, the power line noise appears as low frequency ripples in the image. A schematic of the phase-locked loop, PLL, circuit used for synchronization is available upon request. The amperometric data acquisition complete signal (*A SECM Done*) triggers the PLL synchronizer. The PLL synchronizer then emits a trigger pulse (*Mains Sync*) that occurs within 16 ms (for 60 Hz North American power) of the *A SECM Done* pulse and is located at a specific phase with respect to the *Mains Current*. *Mains Sync* is

used to trigger an analog sweep generator built into the SECM bipotentiostat (EI-400, Ensman Instrumentation, Bloomington, IN) and also data acquisition of the CV data (*V Sweep and Tip Current*). The resulting CV tip current is digitized and tip movement starts a new sequence. Note that we show a cyclic voltammetry implementation here, but little modification would be required to implement linear sweep, potential step, or ac methods of potential excitation.

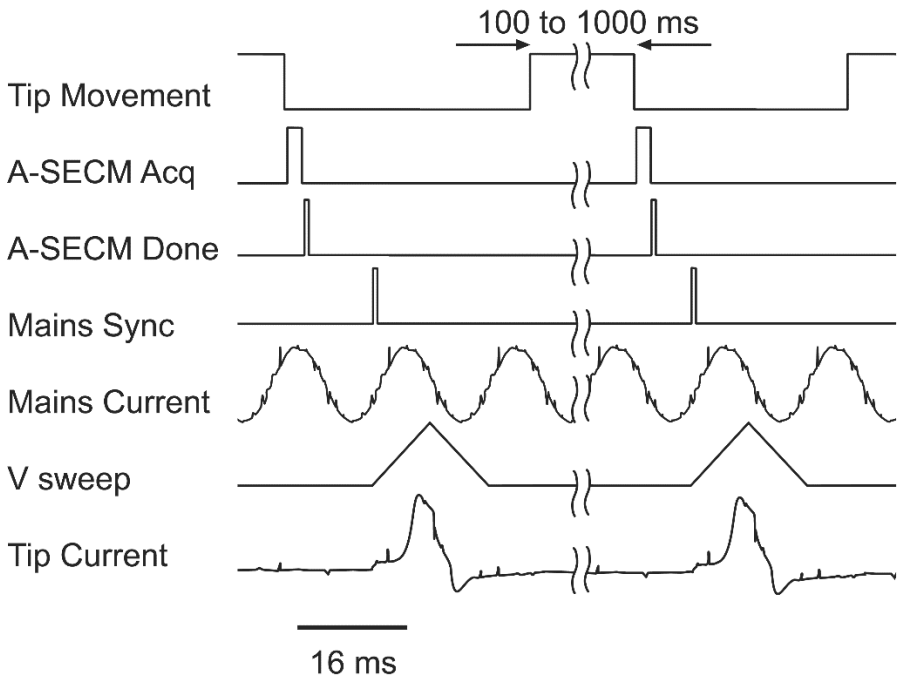

FIGURE 1. Timing diagram showing the tip-movement and data-acquisition sequence for the FSCV-SECM experiment.

Single vertical or horizontal line scans can be recorded using the above procedure. For images, the tip is scanned along the *major* axis, returned to the start position, and is incremented in the *minor* axis for each line of image data. Images are made either by scanning vertically in the X-Z (or Y-Z) plane or horizontally in the X-Y plane (Figure 2). The tip position scan rate is affected by the time required to acquire the voltammogram but this is compensated by changing the actual tip movement speed. For example, an image nominally acquired at a tip movement

speed of 10 μm/s and resolution of 1 μm would use a position step 100 ms long. However, the voltammetric signal adds a delay. A 0.8 V sweep at 100 V/s takes 16 ms and the average delay for the PLL synchronization (in North America) is about 8.4 ms. Thus, our effective tip movement speed is 1μm/0.124s or 8 μm/s. If desired, the effective tip movement velocity is adjustable by changing the actual tip movement speed, in this case to 12.4 μm/s.

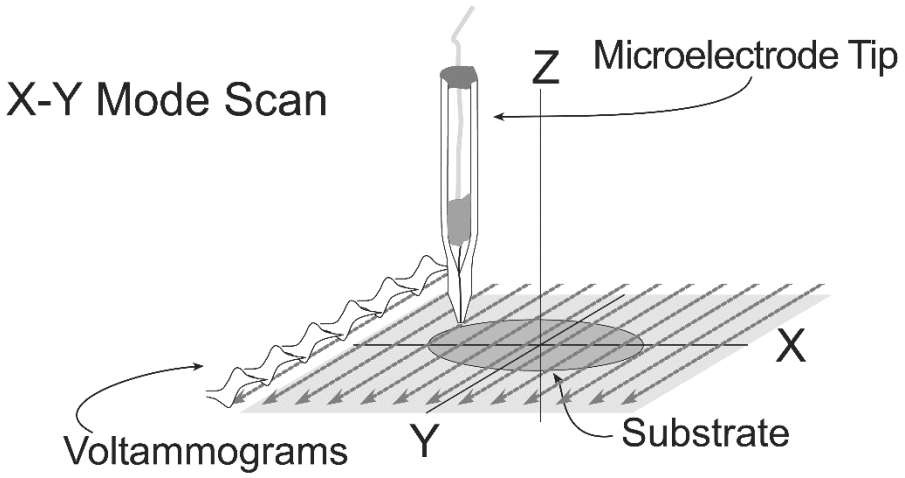

FIGURE 2. Illustration of the data collection sequence with the FSCV-SECM. Each raster line of data is composed of a sequence of voltammograms recorded at regular intervals along the raster line. The illustration here shows a typical X-Y horizontal imaging mode. Similarly, a vertical X-Z (or Y-Z) image is obtained using vertical raster lines.

A schematic illustration of the FSCV-SECM instrument is shown in Figure 3. Changing between A-SECM operation and V-SECM modes requires minimal hardware changes since our potentiostat (like most) can readily scan at CV rates of 100 V/s and higher. The positioner uses a closed-loop Burleigh Inchworm™ based system (6200 ULN) to provide accurate and precise movement at submicrometer resolution. As indicated in the schematic diagram, separate data channels are used to record the rapid voltammetric currents and potentials and the lower

frequency signals of the amperometric data. A set of simple low-pass filters were also introduced, which allows simultaneous acquisition of low and high frequency amperometric and voltammetric data. The tip (T) current (and substrate (S) current in bipotentiostatic operation) is transduced and amplified by the potentiostat. The potentiostat has an internal low pass filter (lpf) set at a value such that $RCnv$ = 4 mV, where RC is the filter time constant (s), n is the number or electrons in the CV wave, and v is the CV scan rate (mV s^{-1}). This is optimal for acquiring CV data without significant distortion due to the low pass filter, lpf [28, 29]. At 100 V/s the filter is set to ~4 kHz and serves the dual role of reducing noise and acting as an anti-aliasing filter for the analog-to-digital converter (ADC). The tip signal is sent to one channel of the ADC and also to a second lpf with an 8 Hz cutoff frequency. The output of this second filter is routed to a separate channel of the ADC. The second filter is used to reduce noise when recording amperometric signals. The setup was slightly modified for Cl^- imaging: the CVs were run during the forward and backward tip scans with the same time between CVs: 300 ms ± 30 ms. The tip raster rate was calibrated to set the time between CVs with the scan rate and tip steps. Experiments in quiescent solutions were performed with a digital oscilloscope (TDS 540A, Tektronics, Beaverton, Oregon).

Data Display The V-SECM image current data is a function of three independent variables, two spatial (e.g. x and y) variables and the voltammetric time, τ, or potential – $E(\tau)$ – variable. Methods used in displaying conventional A-SECM images can be adapted to display V-SECM data if a 3D data subset is extracted from the 4D data. As such, images are made by displaying the tip current versus the spatial variable at a constant experiment time, τ, (or voltage) from the CV sweep. Thus, the image is a function of, e.g., x, y, and $E_{tip}(\tau)$. Compare to A-SECM images, which are functions of, e.g., x, y, and E_{tip}, where E_{tip} is constant. Displaying the complete 4D set is possible using animation to plot an ordered series of successive 3D slices of the 4D set.

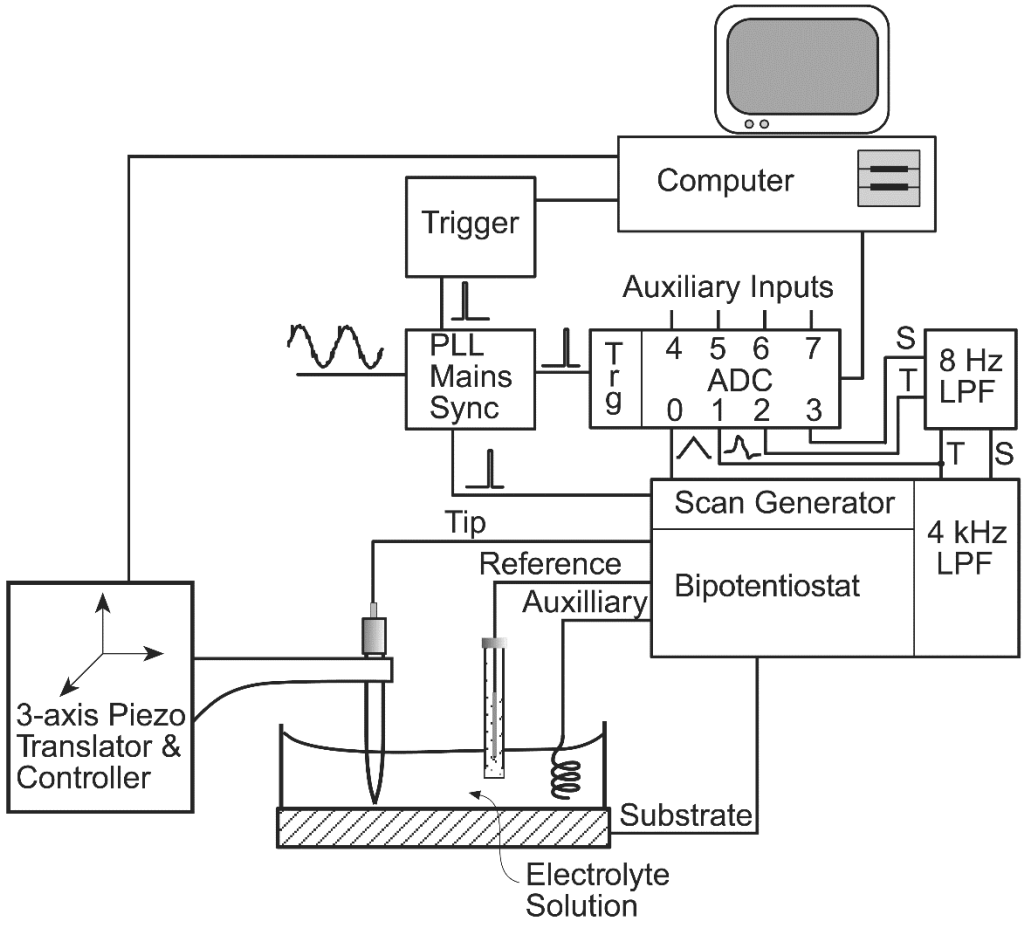

FIGURE 3. Schematic diagram of the FSCV-SECM instrument.

RESULTS AND DISCUSSION

Fast-Scan CV SECM with N,N-Dimethyl-1,4-phenylenediamine (DMPPD) Mediator An initial experiment with use of the FSCV – SECM instrument in the V-SECM mode of imaging employed a microdisk substrate and the reduced compound N,N-dimethyl-1,4-phenylenediamine (DMPPD) as mediator. The SECM images with this mediator will begin to highlight the differences between A-SECM and V-SECM.

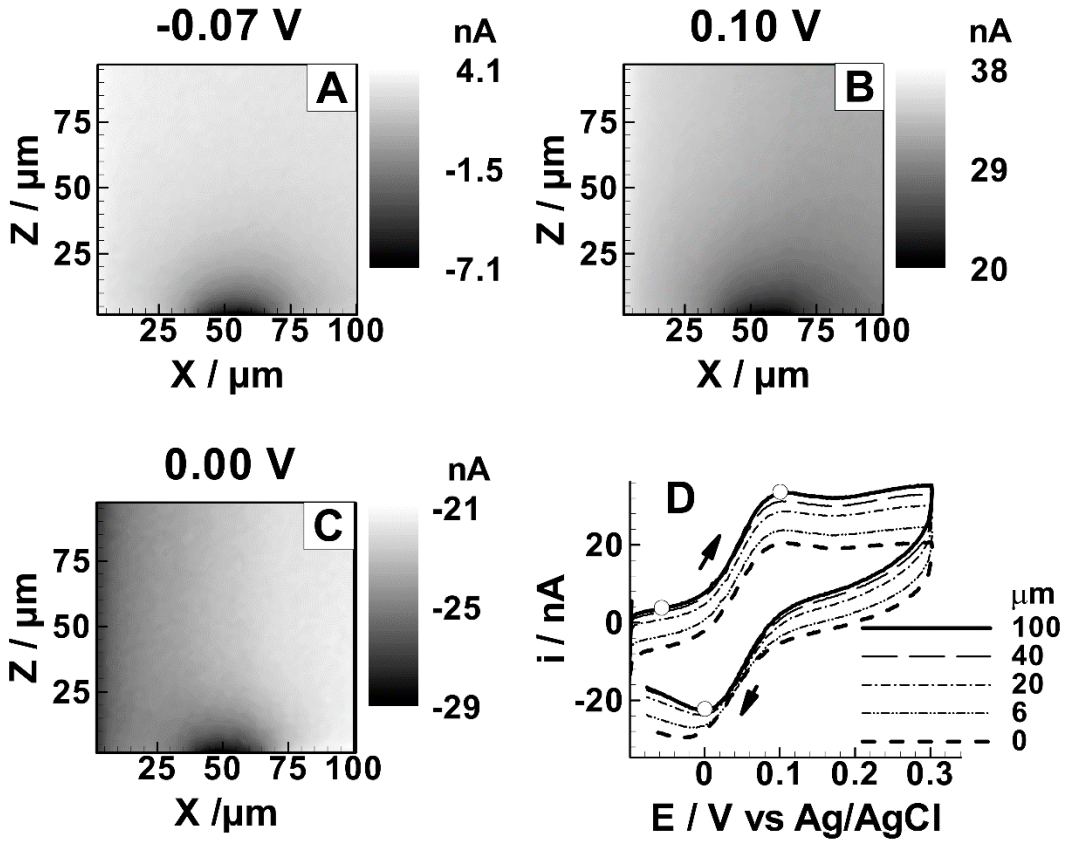

FIGURE 4. (A-C) SECM images extracted from a single vertical (X-Z) FSCV-SECM data set. Each image is generated at a specific tip potential (i.e $E_{tip}(\tau)$) as marked by the open circle on the voltammograms in (D). (D) Voltammograms extracted from the FSCV-SECM data set at an X coordinate of 55 µm (the substrate center) and at the vertical tip-substrate separation as indicated. The mediator is 1 mM DMPPD in 0.25 M K_2HPO_2 + 1 M KCl (pH 10). The tip is a 10 µm diam Pt and the substrate is a 25 µm diam Pt electrode biased at 0.40 V vs Ag/AgCl. The tip CV scan rate is 100 V/s and the nominal imaging scan rate is 20 µm/s.

For these images, a potential of 0.40 V vs Ag/AgCl is applied to the 25 µm diam Pt substrate, which is sufficient to oxidize the DMPPD. The oxidation of DMPPD is a $2e^-$, $1H^+$ reaction at the electrode surface. Oxidation is followed by an irreversible deamination reaction of the imine with OH^- to form quinoneimine [30-32]. The sub-images shown in Figures 4A-C are extracted from a

data set produced from a *single* X-Z FSCV-SECM scan. For example, Figure 4A is generated by plotting all currents corresponding to the tip potential of -0.07 V from the *forward* sweep of the CV (see the open circle position on Figure 4D). The image data set was acquired with a voltammetric sweep rate of 100 V/s at a 10 μm diam Pt tip in an aqueous solution of 1 mM DMPPD at pH 10 (0.25 M K_2HPO_4 + 0.1 M KCl). Figure 4D shows a set of extracted CVs taken from the FSCV-SECM data set corresponding to the tip-substrate separation as marked and at a constant X position corresponding to the center of the substrate electrode (i.e. X = 55 μm).

The CV in Figure 4D at 100 μm is representative of the CVs obtained in bulk solution. Martin and Unwin have determined that the second-order rate constant for the reaction of the imine with OH^- is 1.0×10^4 L mol^{-1} s^{-1} [32]. At constant pH, the chemical reaction is pseudo first order and is an example of an E_rC_i (electrochemically reversible, chemically irreversible) mechanism conveniently adjustable with pH. As seen, the CV is nearly chemically reversible at 100 V/s and is consistent with the relatively slow chemical reaction at pH 10.

Interpretation of the data in Figure 4 proceeds by noting that the tip is held at an initial potential of -0.10 V and, except for the brief voltage excursion during the tip CV, is constantly reducing the substrate-produced imine, producing a net reductive current. This baseline signal is the current that would be observed in an A-SECM experiment with the tip at -0.10 V. Thus the image of Figure 4A at a potential of -0.07 V, located at the foot of the CV wave, is similar to that observed at an A-SECM experiment and can be similarly related to the concentration of DMPPD (the relationship between concentration and current is nonlinear due to the SECM feedback effect [33]). Note, however, that there are additional current components in FSCV-SECM images due to the background or charging currents when compared to A-SECM images. The compact concentration zone for the imine in Figure 4A extends out about 20 μm from the substrate electrode. Given the rate constant for reaction with OH^-, the half-life of the imine is about 0.7 s. Thus, half of the imine will decay within a diffusion distance of 30 μm as calculated from

$(2Dt)^{1/2}$, where D is the diffusion coefficient for DMPPD (7.2×10^{-6} cm^2/s in alkaline solution) [31].

Figure 4B, acquired at the peak of the DMPPD oxidation wave, apparently shows a lower concentration of DMPPD above the substrate, increasing at larger distances. The current at the DMPPD oxidation wave must come from two sources: oxidation of the tip-reduced imine and DMPPD from the bulk solution. Near the substrate the concentration of DMPPD is depleted by the substrate oxidation but is supplemented by reduction of imine at the tip prior to the CV scan. The oxidation of the tip-reduced imine produces the majority of the image contrast near the substrate. The remainder of the contrast is due to the concentration gradient of DMPPD exending from the substrate electrode into the bulk.

Figure 4C, derived from the cathodic peak corresponding to imine reduction, can be understood from Figure 4B. Since the CV peak for DMPPD is nearly reversible at this scan rate, the image is effectively the inverse of the image formed from the anodic peak (Figure 4B).

In both Figures 4B and 4C, the current decreases from left to right along the X axis. This can be understood as a time-dependent phenomenon. The images are acquired by first scanning the tip towards the surface along the Z axis and then stepping along the X axis for the next raster. Thus, the left side of the image is at the beginning and the right side is acquired at the end of the image acquisition (i.e. about 10 min total acquisition time). It is likely that the shading is due to a small loss of activity with time, which would reduce the peak current or shift the peak potential. DMPPD oxidation is known to cause electrode filming and subsequent loss of activity [30]. No shading is noted in Figure 4A, since this image is from a steady-state reductive current and is relatively insensitive to the small kinetic effect produced by electrode filming. An alternate hypothesis, that DMPPD is undergoing bulk concentration depletion due to the substrate electrolysis, is discounted since it would produce a left-right shading in Figure 4A.

These results show that FSCV-SECM images produce potential-resolved image data that is qualitatively similar to results that can be obtained by GC SECM imaging with A-SECM. However, the FSCV-SECM data may provide superior information about causes of image degradation due to the additional information acquired in the voltammetric data (e.g. peak shifts)

Fast-Scan CV SECM with 4-Acetamidophenol Mediator 4-Acetamidophenol (APAP, acetominophen) is oxidized in a chemically irreversible two electron, two-proton process to N-acetyl-*p*-quinoneimine (NAPQI), Eq. (1), which is in equilibrium with its acid form ($NAPQIH^+$), Eq. (2).

$$APAP \rightarrow NAPQI + 2e^- + 2H^+ \quad (1)$$

$$NAPQI + H^+ \rightleftharpoons NAPQIH^+ \quad (2)$$

$$NAPQIH^+ + H_2O \rightarrow \text{hydrated-NAPQI} + H^+ \rightarrow BQ + -CH_3COH_2 \quad (3)$$

In acid solution, $NAPQIH^+$ hydrates (hydrated-NAPQI) and then decomposes to benzoquinone (BQ) Eq. (3) [34]. Under the conditions here, the initial EC reaction is rapid compared to the following reaction to form BQ. Use of this mediator illustrates the ability of the FSCV-SECM technique to produce chemical maps of multiple species in a single imaging scan.

Figure 5 show results from an X-Z FSCV-SECM scan in a 2 mM APAP in 1.8 M H_2SO_4 solution. During imaging, the 12 µm diam Au tip is scanned at 100 V/s from 0 to 1.2 V. The substrate is an embedded 100 µm diam disk Au electrode biased at 1.2 V. Figure 5A shows a set of extracted voltammograms from a single FSCV-SECM data set that illustrates the change in voltammetry with distance as the tip is positioned at various distances above the substrate. A peak for the APAP oxidation is seen at 0.78 V, while a small reverse peak is observed at 0.72 V, indicating at this scan rate, the reaction is beginning to become chemically reversible. A pair of

peaks at 0.49 and 0.55 V correspond to the reduction of BQ and the oxidation of hydroquinone (HQ), respectively, Eq. (4).

$$BQ + 2H^+ + 2e^- \rightleftharpoons HQ^+ \quad (4)$$

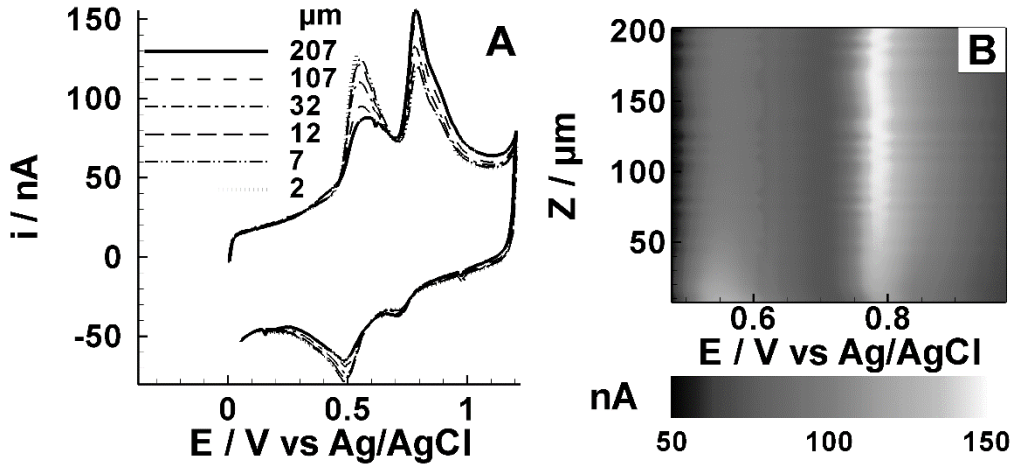

FIGURE 5. Two views of extracted FSCV-SECM data taken from a single vertical (X-Z) scan above disk substrate. (A) Voltammograms at the indicated tip-substrate separation. (B) A 2-dimensional gray-scale plot showing the tip current from a portion of the positive-going branch of the CV versus the vertical tip position. The mediator is 2 mM APAP in 1.8 M H_2SO_4. The tip is a 12 μm diam Au and the substrate is a 100 μm diam Au electrode biased at 1.20 V vs Ag/AgCl. The tip CV scan rate is 100 V/s and the nominal imaging scan rate is 20 μm/s.

At the substrate potential, APAP is oxidized at its diffusion-controlled rate and, since the potential is continuously applied to the substrate throughout the experiment, there is a buildup of the ultimate reaction product (BQ) near the substrate. The presence of a HQ wave can be explained by noting that the tip is initially biased at 0.00 V and is, therefore, reducing BQ to HQ prior to the CV transient. Figure 5B is a gray-scale plot of all the currents from a portion of the positive-going branch of the CV versus the Z position and shows the increase in APAP

concentration (at 0.78 V) and decrease in HQ concentration (at 0.55 V) moving away from the substrate.

Figure 6 shows a comparison of A-SECM and FSCV-SECM X-Y images made with APAP mediator under the same condition as Figure 5. Figures 6A-C are extracted SECM images from a single horizontal (X-Y) FSCV-SECM data set and correspond to images made near the CV peaks for HQ, APAP, and BQ species, respectively. Each chemical species produces a different image, most clearly shown by the increase in current over the substrate in Figure 6A from HQ oxidation and a decrease in current from depletion of APAP in Figure 6B. In contrast to these V-SECM images, Figure 6D is an A-SECM image collected in the process of collecting the FSCV-SECM image. Unlike the others, this image is based on positive feedback and not generation/collection.

Note the apparent shift along the X-axis of the position of the minimum or maximum of the current in Figures 6A-D. Since all images are acquired simultaneously, explanations due to drift in the piezo positioners cannot be invoked. Figures 6A and C show an image shift to the right, which is readily understood to arise from the continuous production of BQ during the image acquisition, which proceeds from left to right. This buildup of BQ concentration produces a sloping background and pushes the maximum to the right, as seen in the figures. In Figure 6B, the current minimum is shifted to the left, this is explained by noting that the APAP wave is on the diffusional tail of the HQ oxidation wave, and the increasing BQ concentration will effectively increase the current at the APAP peak with time, shifting the apparent minimum to the left. Figure 6D shows a current maximum in-between the others. In addition, the feature shape is smaller, corresponds to the substrate dimensions, and is more symmetrical than the other images. In considering what we have learned from the other image data, Figure 6D is based on positive

feedback, not from APAP and NAPQI but from the reaction product BQ. The tip produces HQ from BQ and the substrate is able to rapidly oxidize the HQ, setting up the positive feedback loop.

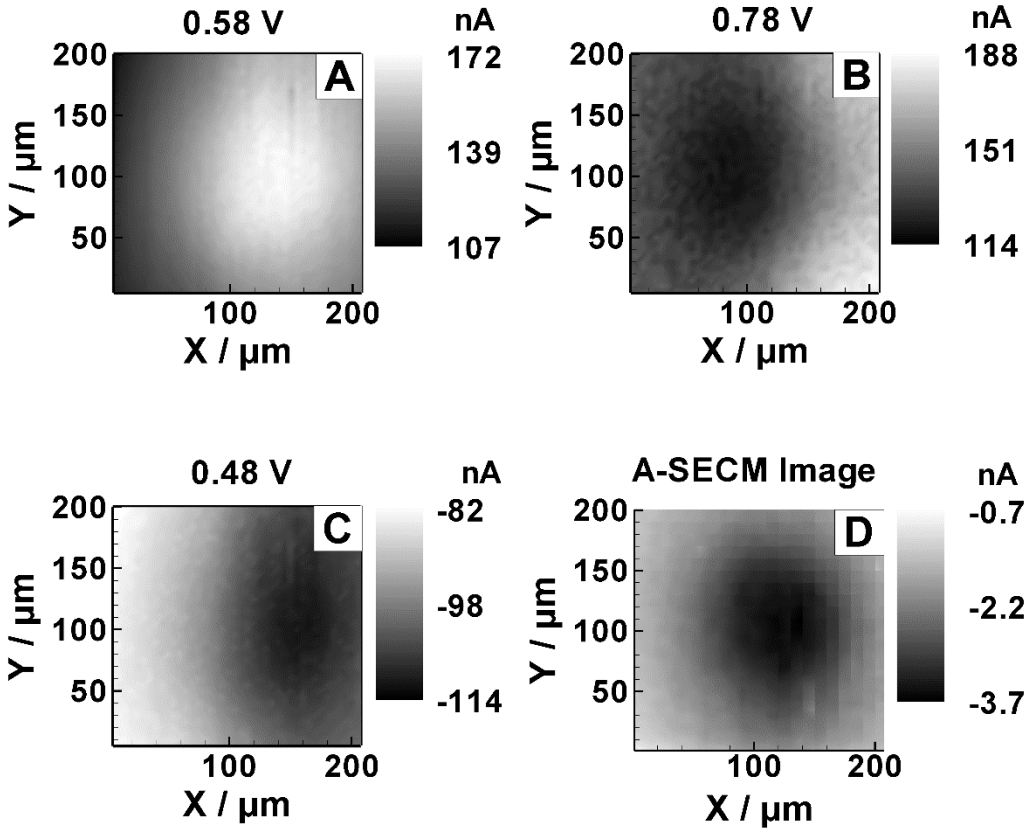

FIGURE 6. (A-C) SECM images extracted from a single horizontal (X-Y) FSCV-SECM data set. Each image is generated at a specific tip potential (i.e $E_{tip}(\tau)$) as noted above each image. The mediator is 2 mM APAP in 1.8 M H_2SO_4. (D) A-SECM image acquired simultaneously to the data in A-C. The tip potential is that of the initial potential of the CV scan, 0.0 V. Note the difference in current scale. The tip is a 12 µm diam Au and the substrate is a 100 µm diam Au electrode biased at 1.20 V vs Ag/AgCl. The tip CV scan rate is 100 V/s and the nominal imaging scan rate is 20 µm/s at a tip-substrate separation of about 3 µm.

It should be noted that the image shifts noted here are not unique to this experiment but would be found in any generation/collection SECM experiment. The difference here is that the effect can be readily recognized as an effect of the follow-up chemical reaction due to the additional information given by the CV data.

The results of this experiment demonstrate that simultaneous images of several chemical species can be obtained in a single FSCV-SECM scan. In contrast to the limited information obtained by a single A-SECM image, the sub-images derived from a single FSCV-SECM scan clearly show the presence of different chemical species during the oxidation of APAP. A common difficulty with conventional A-SECM images is that the current measured at a given potential may be a consequence of several redox processes. In the A-SECM image, the net reduction current at the tip is primarily due to the reduction of chemically generated BQ and not from the electrochemically generated NAPQI. In the absence of foreknowledge of the reaction mechanism or multiple A-SECM images, the source of the tip current would likely be incorrectly ascribed to that of the oxidized mediator. However, the FSCV-SECM data provide direct evidence that the reaction is not a simple electron transfer. Moreover, the FSCV-SECM imaging process provides an A-SECM image without requiring a separate scan, thus allowing the the CV-SECM data to be directly compared to the A-SECM data.

Fast-Scan Cathodic Stripping Voltammetry – SECM The use of a voltammetric imaging mode permits image modes that are infeasible with standard A-SECM. For example, images of nonelectroactive species based on changes in double-layer capacitance or images based on adsorption processes. We demonstrate this by using a cathodic stripping voltammetry SECM technique (CSV-SECM) to image Cl^- concentration profiles. In CSV, the formation of adsorbed Hg_2Cl_2 at the surface of a Hg electrodes followed by a cathodic sweep can be used to determine Cl^- [35].

Imaging in the CSV-SECM mode required changing the conditions usually used in the CSV method. Normally the potential is held at a positive value to preconcentrate Cl^- on the surface through the formation of calomel Eq. (5):

$$2Hg + 2Cl^- \rightleftharpoons Hg_2Cl_2 + 2e^- \quad (5)$$

However, using a preconcentration time under the conditions reported here quickly dissolved the Hg film on our tips (in 0.5 M KNO_3) or produced very broad stripping peaks at 100 V/s (in 10 mM H_2SO_4). This is consistent with what Harman et al. reported [36]. In our method the preconcentration step is eliminated and the tip potential is held sufficiently negative to prevent calomel formation during tip movement. When a voltammogram is acquired during imaging, the potential is swept anodic into a potential region where oxidation of mercury to calomel may occur. In experiments in 10 mM H_2SO_4 electrolyte (Figure 7) the potential is initially held at -0.6 V vs MSE and then swept in the anodic direction until the scan reaches a switching potential value of 0 to -0.2 V; then the sweep is reversed in direction and the electrode potential is returned to the initial value. Under these conditions, stable stripping voltammograms were obtained for up to an hour in quiescent solutions, which is greater than the time scale of our imaging experiments.

Since Cl^- is collected as Hg_2Cl_2 only during the voltammetric sweep, the switching potential of the voltammogram is a significant parameter affecting the shape of the CSV peaks. When the switching potential is 0 V vs MSE, cathodic stripping peak heights were proportional to concentration in the range of 0.5 – 10 mM KCl. However, the peak shape and potential changed with Cl^- concentration, due to the higher local Cl^- concentration temporarily produced near the surface of the electrode as Hg_2Cl_2 is reduced (data not shown). This effect is minimized when the switching potential is changed to -0.2 V vs MSE (Figure 7B), which is near the beginning of the Hg_2Cl_2 formation and, thus, lowering the amount produced. Under this condition, the stripping peak potential did not shift as much and the peak height was found to be proportional to

concentration in the range of 1 – 20 mM KCl (Figure 8). For imaging purposes, a constant peak potential value allows straightforward detection of a Cl^- consuming/producing region on a substrate.

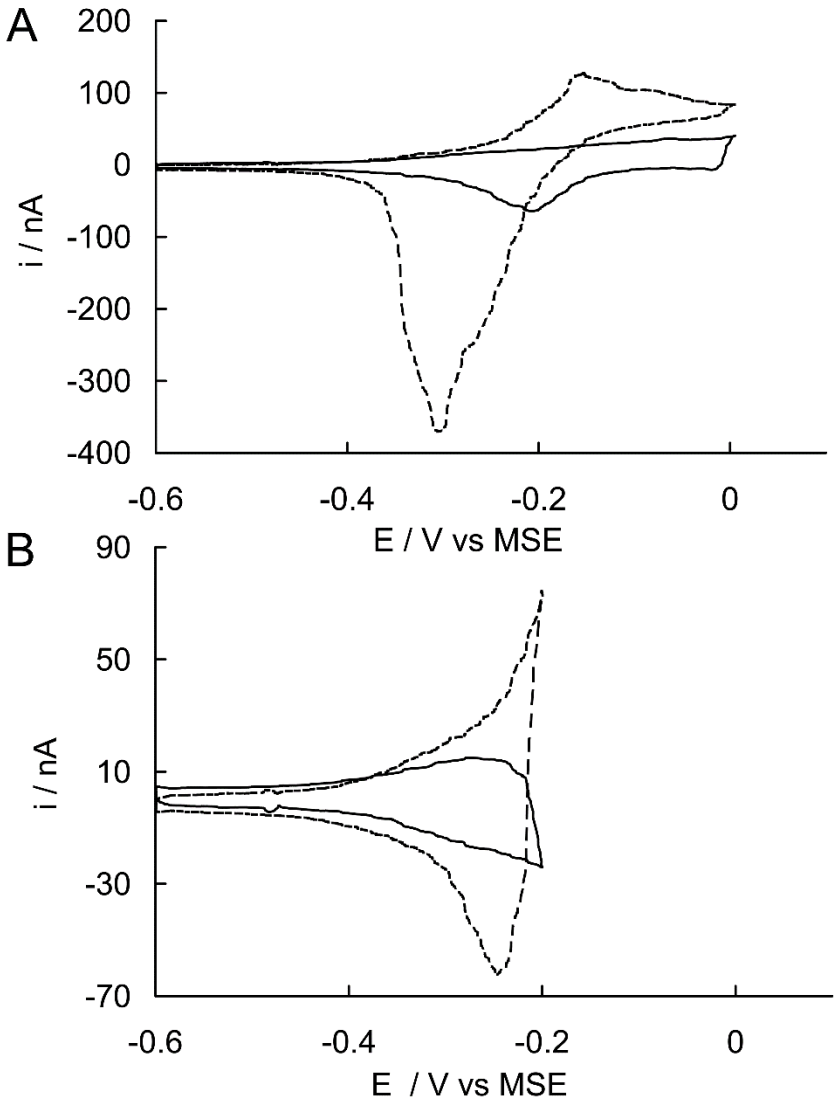

FIGURE 7. Cathodic stripping voltammograms, 5 mM (- - -) and 1 mM (—) KCl/10 mM H_2SO_4 solution at a sweep rate of 100 V/s and with switching potentials of (A) 0 V and (B) -0.2 V vs. the mercury sulfate electrode (MSE)

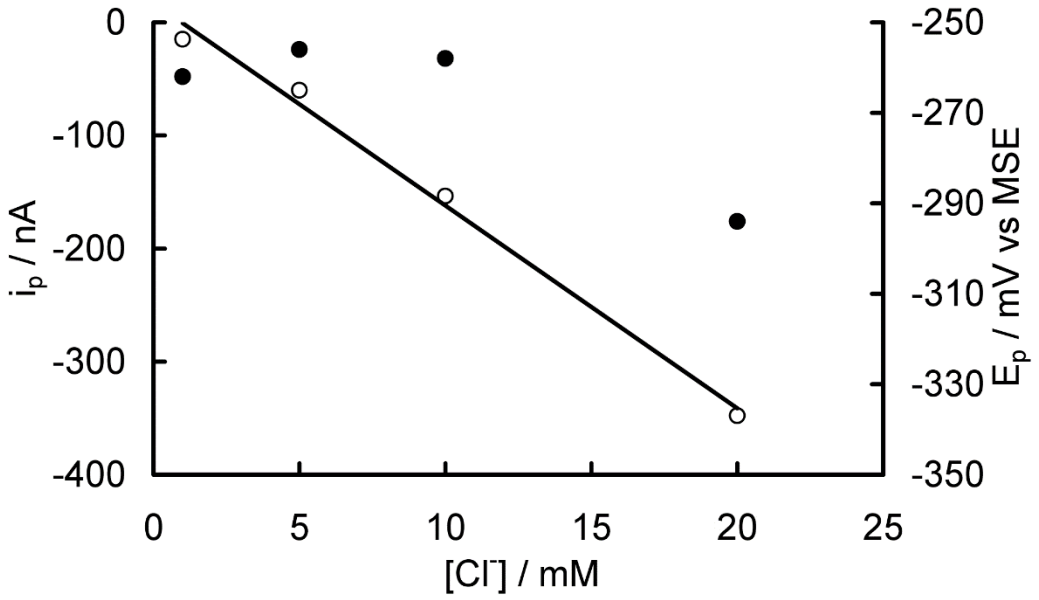

FIGURE 8. CSV peak current (○) and peak potential (●) versus [Cl^-] in 10 mM H_2SO_4 solution. The data were acquired at 100 V/s with a switching potential of -0.2 V vs. MSE.

The ability of the method to map Cl^- concentration is demonstrated here. A localized concentration of chloride ions was produced by reduction of trichloroacetic acid (TCA, Eq. (6)) at a 25 μm diam Au substrate in a Cl^- free citrate-phosphate buffer (McIlvaine, pH 7).

$$Cl_3CCOO^- + H_2O + 2e^- \rightarrow Cl_2CHCOO^- + OH^- + Cl^- \quad (6)$$

Figure 9A is an image obtained by scanning the tip in the x-z plane above the center of the Au electrode substrate in 10 mM TCA/pH 7 buffer. The substrate potential was sufficient to reduce TCA at its diffusion limited rate (-1.5 V vs MSE) making the local concentration of Cl^- ca. 10 mM near the Au electrode. A voltammogram from -0.6 to -0.2 was acquired every 3 μm in the X direction (10 μm/s) and 1 μm in the Z direction (5 μm/s). The image was formed by plotting the peak stripping current at the tip potential of -0.2278 V vs MSE. The Cl- concentration profile

for the region mapped in Figure 9A shows the expected higher concentration of Cl^- above the Au-electrode and diffusion away from the electrode with distance.

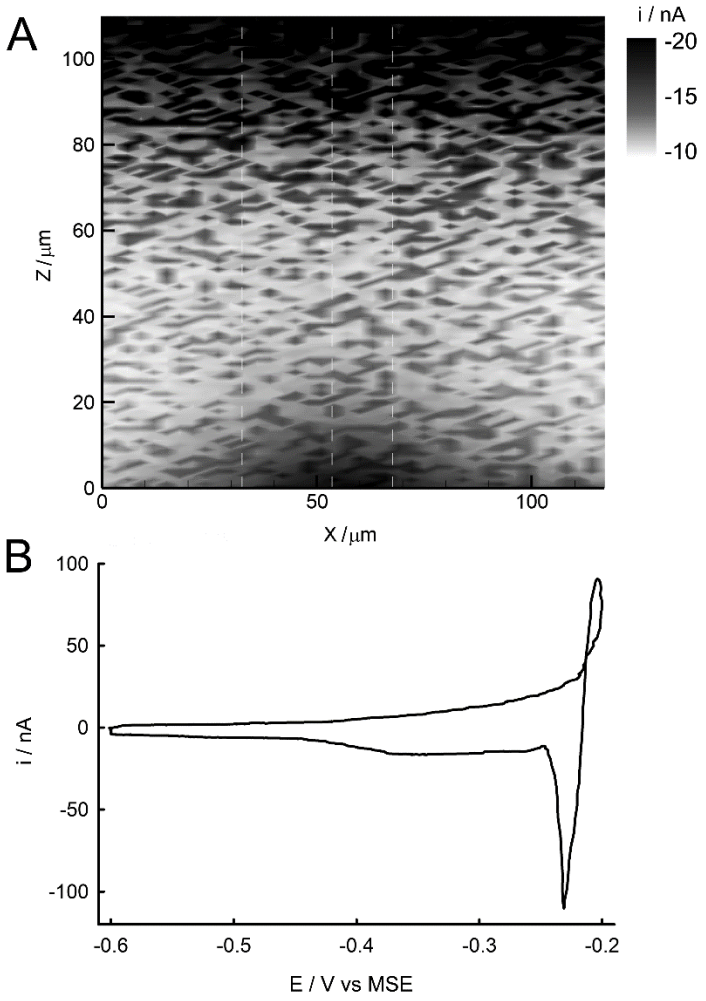

FIGURE 9. (A) SECM image extracted from a single vertical (X-Z) CSV-SECM data set above a 25 μm diam Au disk substrate set to reduce 10 mM TCA in pH 7 buffer. The image is formed from the peak current at the potential of the cathodic stripping peak (-0.2278 V). The vertical dashed lines are at the location for the concentration profiles shown in Figure 10. The image was acquired with 3 μm steps at 10 μm/s in the X direction and 1 μm steps in the Z direction. (B) A CSV acquired in 1 mM KCl/10 mM TCA/pH 7 solution before the image in (A). For (A) and (B) the tip is a 10 μm diam Hg coated, Pt disk swept from -0.6 to -0.2 V vs MSE at 100 V/s.

A preliminary voltammogram obtained in a Cl^--spiked test solution (0.1 mM KCl/ 10 mM TCA/ pH 7 buffer) shows a clear stripping peak (Figure 9B) but appears different than the voltammogram acquired in 10 mM H_2SO_4 (Figure 7). In TCA/buffer solution, the oxidation of Hg has shifted to more negative values while the calomel reduction has shifted in the opposite direction consistent with the presence of some competing complexating process. There is also a change in the charging current and the reverse wave crosses over the forward scan current suggesting modification of the Hg surface. Note that the stripping current in the test CV is larger than those in the image even though the maximum Cl^- concentration should be larger in the image. Also, note that the currents during imaging experiment also decay slowly during the initial part of the image (acquired by scanning left to right, top to bottom on the figure) but eventually reach a stable level at around z < 80 μm.

To demonstrate that the image is a true representation of the concentration map of Cl^-, the currents can be compared to the theoretical concentration profiles at an UME operating at its diffusion limited rate. Eq. (7) was derived by Saito [37] for C_{ox}/C_{ox}^* in cylindrical coordinates:

$$C_{ox}^* - C_{ox} = \frac{2C_{ox}^*}{\pi} \arctan \frac{a}{\sqrt{\frac{1}{2}\left\{\left(r^2 + z^2 - a^2\right) + \sqrt{\left(r^2 + z^2 - a^2\right)^2 + 4z^2a^2}\right\}}} \qquad (7)$$

From this, the concentration of the product of the reaction, i.e., $[Cl^-]$ can be derived using the equimolar conditions (reaction 6) and setting $C_{Cl} = 1 - C_{ox}$, which holds at every (r, z) position. This equation was used to compare concentration profiles (constant *r*) with experimental stripping data (Figure 10). The normalized data fits to the theoretical behavior for three different regions in Figure 9A (note the dashed lines indicating these regions). The data was corrected for background, normalized to $i_{t,\infty}$ and added to a *z* offset to account for the uncertainty in the tip-sample distance and tilt. Despite high noise in the experimental data, good agreement was observed for the experiment and the theoretical values. The stripping currents are thus consistent

with the theoretical map of an UME producing Cl^- from the diffusion limited rate of TCA reduction. The noise does indicate that we are working near our lower limit of detection. Future optimization of our experimental method should increase the signal-to-noise ratio and decrease the limit of detection.

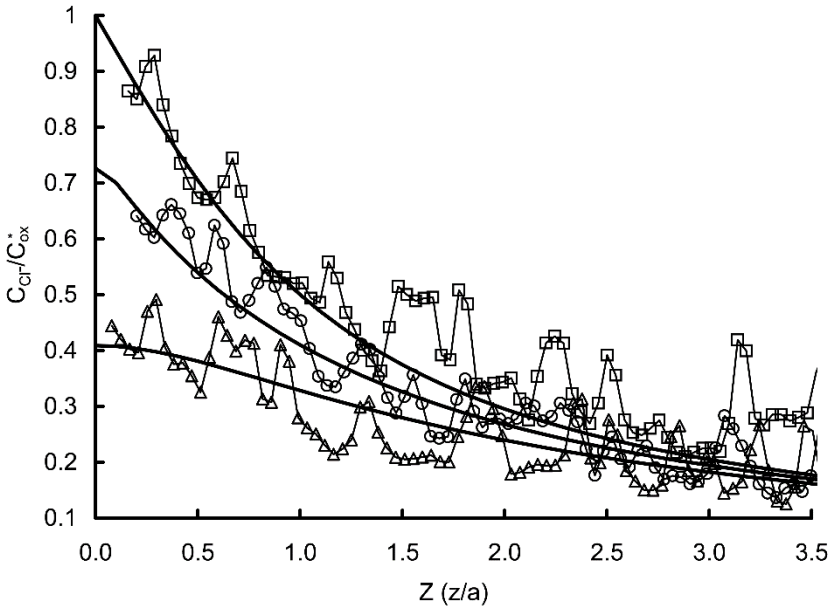

FIGURE 10. A set of experimental and calculated Cl^- ion concentration profiles. Calculated z-profiles for the dimensionless radial coordinate R (r/a) = 0, R = 1.1, R = 1.67, top to bottom, respectively. Normalized experimental profiles (cf. Figure 9) for (□) R = 0, (○) R = 1.1, (Δ) R = 1.67.

CSV has been shown to image variations of Cl^- concentration despite the experimental hurdles described above. These make this experiment a good model for complex systems (e.g. corroding samples or biological substrates) where solution composition is very likely to cause similar complications. In summary, this system is a proof of concept of using adsorption

stripping currents to detect ions in solution. We expect that this method can be readily adapted to image other mercury complexing ions (e.g. other halides or sulfides).

CONCLUSIONS

The selectivity of cyclic voltammetry and the spatial resolution of the SECM have been joined to form a new imaging process that increases imaging efficiency and information available in a scan. The resulting four-dimensional data set can be used to expand the type of images produced with the SECM technique. Most significantly, images of multiple chemical species can be acquired in a single scan as demonstrated by the simultaneous production of concentration maps of HQ, APAP, and BQ during the oxidation of APAP at a substrate electrode. In addition, the use of a voltammetric excitation opens up imaging modes that are not feasible in A-SECM, such as producing images of complexing agents, changes in double-layer capacitance, or adsorption phenomena as demonstrated here in the CSV-SECM images of Cl^- ion concentration.

In the experiments described here, the SECM tip is biased at the initial potential of the CV. This allows us to capture an A-SECM image by collecting steady-state current just prior to the CV transient. The short CV transient time, the time between data points, and the tip movement permits establishment of a solution concentration gradient that is similar to that established in the absence of a CV transient (i.e. normal A-SECM). Our experiments then can be best understood as using the FSCV to probe concentrations at the tip surface as set by the feedback interaction (positive or negative) between the tip and biased substrate. This may be an objectionable complication in some experiments. However, it should be relatively simple to image with an "ac-coupled" amplifier by recording only the transient. This would prevent any effects due to steady-state electrolysis at the tip and allow identification of species by their redox peak position. Also, this complication will not be present in many imaging conditions (such as with insulators) where it will be possible to set the tip electrode potential to avoid any electrolysis at the initial potential.

We feel that the combination of A-SECM and FSCV-SECM will greatly improve the ability to understand SECM images made in complex environments, such as actively corroding alloy materials, catalytic systems, and biological substrates. Further improvements in data collection and analyses, such as use of digital filtering and data subtraction will improve image contrast.

ACKNOWLEDGEMENTS

The authors acknowledge the National Science Foundation for support by grant DBI-9987028. L.D. acknowledges CONACYT for sabbatical support and grant SEP-2004-C01-46197.

REFERENCES

[1] A.J. Bard, M.V. Mirkin (Eds.), Scanning Electrochemical Microscopy, John Wiley & Sons, New York, 2001.

[2] J. Kwak, A.J. Bard, Anal. Chem. 61 (1989), 1221-1227.

[3] A.J. Bard, F.-R.F. Fan, J. Kwak, O. Lev, Anal. Chem. 61 (1989), 132 - 138.

[4] R.C. Engstrom, T. Meany, R. Tople, R.M. Wightman, Anal. Chem. 59 (1987), 2005 - 2010.

[5] R.C. Engstrom, M. Weber, D.J. Wunder, R. Burgess, S. Winguist, Anal. Chem. 58 (1986), 844 - 848.

[6] G. Denuault, M.H.T. Frank, L.M. Peter, Faraday Discuss. Chem. Soc. (1992), 23-35.

[7] M. Etienne, A. Schulte, S. Mann, G. Jordan, L.D. Dietzel, W. Schuhmann, Anal. Chem. 76 (2004), 3682-3688.

[8] K. Tóth, G. Nagy, B.R. Horrocks, A.J. Bard, Anal. Chim. Acta 282 (1993), 239-246.

[9] A. Kueng, C. Kranz, B. Mizaikoff, A. Lugstein, E. Bertagnolli, App. Phys. Lett. 82 (2003), 1592-1594.

[10] J. Kwak, A.J. Bard, Anal. Chem. 61 (1989), 1794-1799.

[11] J.V. Macpherson, P.R. Unwin, Anal. Chem. 73 (2001), 550-557.

[12] M.S. Shin, I.C. Jeon, Bull. Kor. Chem. Soc. 19 (1998), 1227-1232.

[13] D.O. Wipf, A.J. Bard, Anal. Chem. 64 (1992), 1362-1367.

[14] M.A. Alpuche-Aviles, D.O. Wipf, Anal. Chem. 73 (2001), 4873-4881.

[15] A.J. Bard, G. Denuault, C.M. Lee, D. Mandler, D.O. Wipf, Acc. Chem. Res. 23 (1990), 357-363.

[16] R.M. Wightman, D.O. Wipf, Acc. Chem. Res. 23 (1990), 64-70.

[17] R.M. Wightman, D.O. Wipf, in: A.J. Bard (Ed.), Electroanalytical Chemistry, Marcel Dekker, New York, 1989, pp. 267-353.

[18] R.M. Wightman, L.J. May, A.C. Michael, Anal. Chem. 60 (1988), 769A-779A.

[19] R.M. Wightman, C. Amatore, R.C. Engstrom, P.D. Hale, E.W. Kristensen, W.G. Kuhr, L.J. May, Neuroscience 25 (1988), 513-23.

[20] B.R. Scharifker, in: J.O.M. Bockris, B.E. Conway, R.E. White (Eds.), Modern Aspects of Electrochemistry, Plenum Press, New York, 1992, p. 467.

[21] C.C. Hsueh, R. Bravo, A.J. Jaramillo, Brajter-Toth, Anal. Chim. Acta 67 (1997), 349.

[22] D.R. Bull, P. Palij, M.J. Sheehan, J. Millar, J.A. Stamford, Z.L. Kruk, P. Humphrey, J. Neurosci. Methods 32 (1990), 37-44.

[23] P.M. Kovach, A.G. Ewing, R.L. Wilson, R.M. Wightman, J. Neurosci. Methods 10 (1984), 215-27.

[24] S. Hafizi, J.A. Stamford, J. Electroanal. Chem. 319 (1991), 303-310.

[25] D.O. Wipf, A.J. Bard, J. Electrochem. Soc. 138 (1991), 469-474.

[26] L. Diaz-Ballote, L. Veleva, M.A. Pech-Canul, M.I. Pech-Canul, D.O. Wipf, J. Electrochem. Soc. 151 (2004), B299-B303.

[27] L. Veleva, L. Diaz-Ballote, D.O. Wipf, J. Electrochem. Soc. 150 (2003), C1-C6.

[28] D.O. Wipf, E.W. Kristensen, M.R. Deakin, R.M. Wightman, Anal. Chem. 60 (1988), 306-10.

[29] J.L. Anderson, Chem. Instrum. 7 (1976), 25-32.

[30] L.K.J. Tong, K. Liang, W.R. Ruby, J. Electroanal. Chem. 13 (1967), 245-262.

[31] P.R. Unwin, A.J. Bard, J. Phys. Chem. 95 (1991), 7814-7824.

[32] R.D. Martin, P.R. Unwin, J. Chem. Soc. Faraday Trans. 94 (1998), 753-759.

[33] M.V. Mirkin, F.R.F. Fan, A.J. Bard, J. Electroanal. Chem. 328 (1992), 47-62.

[34] J.J.V. Benschoten, J.Y. Lewis, W.R. Heineman, D.A. Roston, P.T. Kissinger, J. Chem. Educ. 60 (1983), 772.

[35] R.G. Ball, D.L. Manning, O. Menis, Anal. Chem. 32 (1960),

[36] A.R. Harman, A.S. Baranski, Anal. Chim. Acta 239 (1990), 35-44.

[37] Y. Saito, Rev. Polar. (Japan) 15 (1968), 178-186.